Journal of Materials Science: Materials in Electronics (2020) 31:10499–10511
https://doi.org/10.1007/s10854-020-03598-y

The influence of Eu^{3+} doping on the studies of luminescent properties and quantum efficiency of $ZnWO_4$ phosphor

Qingju Ning[1] · Cuicui Zhou[2] · Yongsheng Shi[2]

Received: 28 February 2020 / Accepted: 13 May 2020 / Published online: 20 May 2020

Abstract
$ZnWO_4$:Eu^{3+} red nanophosphors have been synthesized by a simple environmentally friendly and low-cost molten salt method. The phase structure, morphology, SAED, photo-luminescent (PL), lifetime, color rendering, quantum efficiency and stability properties of the phosphor were investigated in detail. The XRD results indicated that all Eu^{3+} ions doping $ZnWO_4$ samples crystallize in a single crystal wolframite structure and exhibit superior crystallinity. Under the excitation of 394 and 465 nm, $ZnWO_4$:Eu^{3+} phosphors can be exhibited red light emission. The photoluminescence excitation spectra of $ZnWO_4$:Eu^{3+} phosphors show several emission peaks, on account of the *f–f* transitions of Eu^{3+} ions. The quantum efficiency of $ZnWO_4$:0.07Eu^{3+} phosphors were calculated to be 40.5%, the CIE chromaticity coordinate of $ZnWO_4$:0.07Eu^{3+} phosphors were (0.631, 0.364) closed to the red phosphors standard value (0.670, 0.330), based on the Judd–Ofelt analysis, Judd–Ofelt intensity parameters (Ω_2/Ω_4) includes symmetry of Eu^{3+} ions crystal field environment, it was suggested that $ZnWO_4$:0.07Eu^{3+} phosphors were a potential phosphor in LEDs. This research sheds new light on improving the quantum efficiency, stability properties and CIE chromaticity coordinate.

1 Introduction

With the rapid development of society, people pay great attention to the luminescent material that to strengthen the luminescent properties, a lot of literatures have reported [1] that rare earth ions doping have important applications in luminescent properties. In the tungstate materials [2], Zinc tungstate is special, it is different from other materials, which belongs to a kind of self-activating phosphor, $ZnWO_4$-based materials are divided into single crystal and nanoparticles and so on [3, 4]. Tungstate materials have attracted intensive attention originating from typical merits, such as high light yield, high average refractive index, physical, chemical, and structural properties, which has been widely used in lighting and display devices, including plasma display panels, white light-emitting diodes (WLEDs) [5]. Up to now, one of the main obstacles is improving the stability properties, which can be extremely difficult for its development and commercial in WLEDS.

There are several methods were prepared for the rare earth ions doping in improving the luminescent properties of the phosphor. The literature has reported that Dang Yuan et al. A novel electrochemical sensor for the selective determination of hydroquinone and catechol using synergic effect of electropolymerized nicotinic acid film and Cd-doped $ZnWO_4$ nanoneedle [6], Minzhu Zhao et al. Investigation of energy transfer mechanism and luminescent properties in Eu^{3+} and Sm^{3+} co-doped $ZnWO_4$ phosphors [7], Chen Guiqiang et al. Improving red emission by co-doping Li^+ in $ZnWO_4$:Eu^{3+} phosphors [8], Chai Xiaona et al. Upconversion luminescent and temperature-sensing properties of Ho^{3+}/Yb^{3+}-codoping $ZnWO_4$ phosphors based on luminescent intensity ratio [9], Chunyang Li et al. Color changing from white to red emission for $ZnWO_4$:Eu^{3+} nanophosphors at a different temperature [10], therefore, in this work, the nanocrystals of $ZnWO_4$:Eu^{3+} phosphors have been prepared by the molten salt method.

As it can be observed in the literature [11], Eu^{3+} ions doping frequently play important roles in morphologies as well as in luminescent properties of phosphors. At the same time, it was used for an activator by the rare earth ions doping the phosphors. The purpose of this work are used to investigate

✉ Cuicui Zhou
1135302252@qq.com

[1] School of Materials Science and Engineering, Shaanxi University of Science & Technology, Xi'an 710021, China

[2] College of Electrical Information and Control Engineering, Shaanxi University of Science & Technology, Xi'an 710021, China

the luminescent properties of phosphors, Judd–Ofelt [12] the theoretical analysis, quantum efficiency and stability properties. So far, to the best of our knowledge, there has not yet been any report similar to our work. For the first time, the goal of this work is discussed in detail for the luminescent properties of phosphors and Judd–Ofelt analysis. The contributions of this paper can be summarized as follows better understand luminescent properties, quantum efficiency and stability properties of the sample.

2 Experimental methods

2.1 Preparation of $ZnWO_4$ and $ZnWO_4$:Eu^{3+} specimen

All chemical reagents are analytical reagent (AR) and from Sinopharm Chemical Reagent Co., Ltd. China. All chemicals were utilized without further purification. In brief, all specimens operated at a fixed doping concentration of the Eu^{3+} ions was 7 mol%, Eu^{3+} ions doping $ZnWO_4$ nanophosphors were prepared via the molten salt method. Using analytically pure (AR) $Na_2WO_4{\cdot}2H_2O$ (99.5%), Eu_2O_3 (99.99%) and $Zn(CH_3COO)_2{\cdot}2H_2O$ (99%) as raw materials and $LiNO_3$ (99%)–$NaNO_3$ (99%) as molten salt media. The raw materials $Na_2WO_4{\cdot}2H_2O$ and $Zn(CH_3COO)_2{\cdot}2H_2O$ were weighed out according to the composition of $ZnWO_4$. The molten salt with the weigh ratio about $LiNO_3$:$NaNO_3$ to 1:3 and dissolved. Then, the raw materials were added to the molten salt solution. The mixture of raw materials and molten salt (molar ratio of 1:4), and then placed in a mortar to grind for 30 min, subsequently, the mixture was heated to the target temperature (180 °C) at a speed rate of 5 °C/min and kept for 8 h in the room temperature. After cooling, the solidified melt was washed with distilled water to remove the sodium salt and residual lithium salt. The silver nitrate solution was not tested until a white precipitate was produced, which demonstrated that there was no excess Cl^- in the solution. Ultimately, the obtained specimens were dried at 60 °C for analysis.

2.2 Material characterization

The structure of obtained powders were characterized by X-ray diffraction patterns (XRD, D/max, 2200 PC) at a 2θ range from 10° to 70° with 0.02°/step size with Cu-Kα radiation ($\lambda = 1.5405$ Å). Rietveld refinement of the sample was presented by the General Structure Analysis System software (GASA). The morphologies of samples were observed by field emission scanning electron microscopy (Q45, FEI, America). UV–Vis–NIR spectrophotometer (Cary5000, Agilent, America) was used to record the absorption spectra in the range of 200–800 nm. The Raman spectrum was tested by a microscopic confocal laser spectrometer (Renishaw-invia, Renishaw, Britain). The light source was the laser of an argon ion laser with a spectral resolution of 2 cm^{-1}. XPS (X-ray photoelectron spectroscopy, Axis Supra, Britain) was measured the composition of the elements and oxygen vacancy of the sample. The excitation spectra and emission spectra were detected by Photoluminescence spectrometer (F-4600, Hitachi, Japan) and the decay time was obtained by using the xenon lamp as an excitation source. The quantum efficiency of the phosphors were conducted with a Quantum-QY Plus UV–NIR absolute PL quantum yield spectrometer (C9920-03, Hamamatsu photonics K.K., Japan) with samples in powder form and the temperature-dependent PL spectra were evaluated on Hitachi FLS-980 Fluorescence Spectrophotometer. All the above measurements were performed out at room temperature.

3 Results and discussion

3.1 XRD characterization

The XRD spectra of $ZnWO_4$ phosphor and $ZnWO_4$:0.07Eu^{3+} crystal particles were obtained by the LTMS method in $LiNO_3$–$NaNO_3$ at 8 h. As shown in Fig. 1, it can be observed all the diffraction peaks can be perfectly indexed to monoclinic crystal structured $ZnWO_4$ (JCPDS card No. 15-0774), which demonstrates that the substitution of Eu^{3+} ions have a little modest effect on the crystal structured of $ZnWO_4$. Furthermore, under the same synthesis condition, all the observed diffraction peaks of the $ZnWO_4$ and $ZnWO_4$:0.07Eu^{3+} phosphors are strong and sharp, which implies good crystallinity and observes from the diffraction pattern, this paper found no other secondary and mixed phase in the figure. Therefore, all prepared samples are the monoclinic wolframite structure, as can be observed from

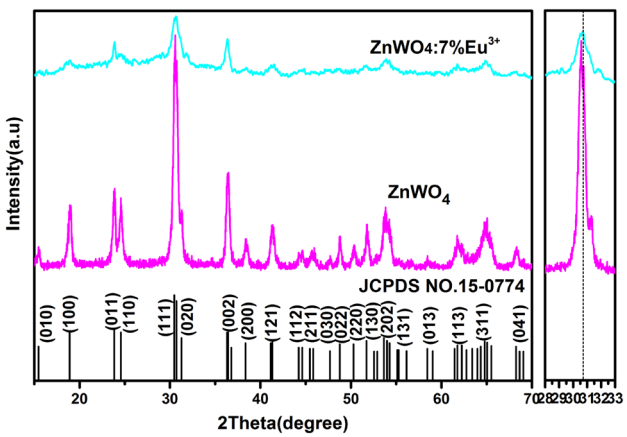

Fig. 1 XRD patterns of the $ZnWO_4$ and the $ZnWO_4$:0.07Eu^{3+}

the partial enlarge from 28º to 33º of the figure. Obviously, it can be noticed that the diffraction peaks of the diffraction pattern shift toward a lower angle deviation due to the Eu^{3+} ions doping which was described to expand the lattice. According to the similar ionic radius and stability of the crystal system, the ion radius of the Eu^{3+} (0.95 Å) is close to the ionic radius of Zn^{2+} (0.74 Å), however, the larger than the W^{6+} (0.60 Å) ions radius. Therefore, the Eu^{3+} ions will preferentially replace the Zn^{2+} position in the $ZnWO_4$ matrix. Based on the Bragg equation:

$$2d \sin\theta = n\lambda \tag{1}$$

where d is the interplanar distance of corresponding crystal plane, θ is the diffraction angle, λ is the wavelength of the X-ray, where n is the number of reflection orders (generally speaking the value of the n is 1), it is interestingly found that with the reduction of the diffraction angle, interplanar distance of corresponding crystal plane becomes larger. According to the above analysis, this may be because the Eu^{3+} ions preferentially replace the Zn^{2+} position in the $ZnWO_4$ lattice, which lead to an increase in the spacing between the crystal faces. The analysis of these results suggests that the sharp and high diffraction peaks with the higher crystallinity of the phosphor. From the crystal structure diagram of the $ZnWO_4$ of the view, ZnO_6 and WO_6 octahedrons are linked to each other by shared oxygen, it can easily conclude that the introduction of Eu^{3+} entered into the $ZnWO_4$ which could bring defects and increase the oxygen vacancies of the surface [13].

3.2 TEM analysis and EDS spectrum analysis

Figure 2 exhibits the SEM images of the (a), HRTEM images of the (b), SAED (c) of the $ZnWO_4$:0.07Eu^{3+} phosphors. The sample has a homogeneous morphology with a diameter of the 7–20 nm which content with the pattern of the XRD. The $ZnWO_4$:0.07Eu^{3+} phosphors with rod-like morphology due to the higher aspect ratio, to clearly understand the crystallinity and purity of the sample by observed the HRTEM. As can be observed in Fig. 2b, the average gap is the lattice fringe of 0.48 and 0.545 nm corresponding to the lattice plane of the (100) and (010) respectively, which further confirmed the formation of the monoclinic structure of wolframite $ZnWO_4$. The SAED figures were shown in Fig. 2c. The picture is consists of a few laps, it is generally accepted that the samples were polycrystalline, it is composed of a lattice, therefore it was concluded that the specimen of a single crystal.

3.3 XPS analysis

To obtain further information on the analysis chemical composition of elements and surface state of the $ZnWO_4$:0.07Eu^{3+} nanorods, the XPS measurements were displayed in Fig. 3. The survey spectrum as illustrated in Fig. 3a, indicating the presence of Zn 2p, W 4f, O 1s, Eu 3d in the as-obtained sample without other elemental signals being observed. With carbon C 1s peak Tag the binding energies (BE) [14]. The XPS peak of C 1s is due to accidental hydrocarbons from the XPS measurement. As can be observed in Fig. 3b, the BE values of C 1s is 284.8 eV, it suggests that the doped Eu^{3+} is trivalent. In the XPS spectrum of Zn 2p, two characteristic peaks located at 1021.88 and 1044.98 eV (Fig. 3c) can be assigned to Zn $2p_{3/2}$ and Zn $2p_{1/2}$, respectively. However, for the pure $ZnWO_4$, Zn $2p_{3/2}$ and Zn $2p_{1/2}$ are centered at 1021.72 and 1044.94 eV. The XPS spectrum of W 4f exhibits two peaks that occurred in 35.38 and 37.48 eV (Fig. 3d), originating from the W $4f_{7/2}$ and W $4f_{5/2}$ of W^{6+}, respectively. Compared with pure $ZnWO_4$, it can easily conclude that there is a shift of 0.63 eV and 0.67 eV to the high binding energy. As displayed in Fig. 3e, crystal lattice oxygen was observed in the peak at 530.88 eV in the Eu^{3+} doping $ZnWO_4$ nanocrystal. In comparison with the pure $ZnWO_4$ phosphor, the BE value of O 1s is 530.71 eV which in accordance with the holding peak of the O^{2-} ion. For the XPS spectrum of Eu 3d, the main two peaks at the binding energies of 1126 and 1155 eV can be ascribed to the Eu $3d_{5/2}$ and Eu $3d_{3/2}$ of Eu^{3+} (Fig. 3f) [15]. The energy of the peaks is 17,145 eV which originated from the Eu $3d_{3/2}$ of the $ZnWO_4$ which in good agreement with the previous work [16]. Based on the above-mentioned analysis results, it can be concluded that the valence C, Zn, W, O and Eu elements are $0, +2, +6, -2, +3$, respectively.

3.4 The ultraviolet–visible reflectance absorption spectra analysis and optical band gap energy analysis

The band structure was conducted by ultraviolet–visible reflectance absorption spectra to investigate the intrinsic electronic of $ZnWO_4$:0.07Eu^{3+} nano-rods (Fig. 4a). In comparison with the band structure of the pure $ZnWO_4$ with the same synthesis, the condition was depicted in Fig. 4a. As can be seen in the picture, Eu^{3+} ions doping the $ZnWO_4$ can strengthen the optical response of the $ZnWO_4$ phosphors, the band gap energy of the phosphors, which the equation is expressed as follows [17]:

$$\alpha h\nu = B\left(h\nu - E_g\right)^{\frac{1}{t}} \tag{2}$$

where α is absorption coefficient, B is the characteristic constant of relating to the material, where $h\nu$ is the photon energy, h is Planck's constant ($h = 4.14 \times 10^{-15}$ eVs). E_g is the optical band gap energy, t is the exponent associated with electron transitions, where $t = 1/2$ is for directly allowed transition, $t = 2/3$ means directly prohibit transitions, $t = 2$

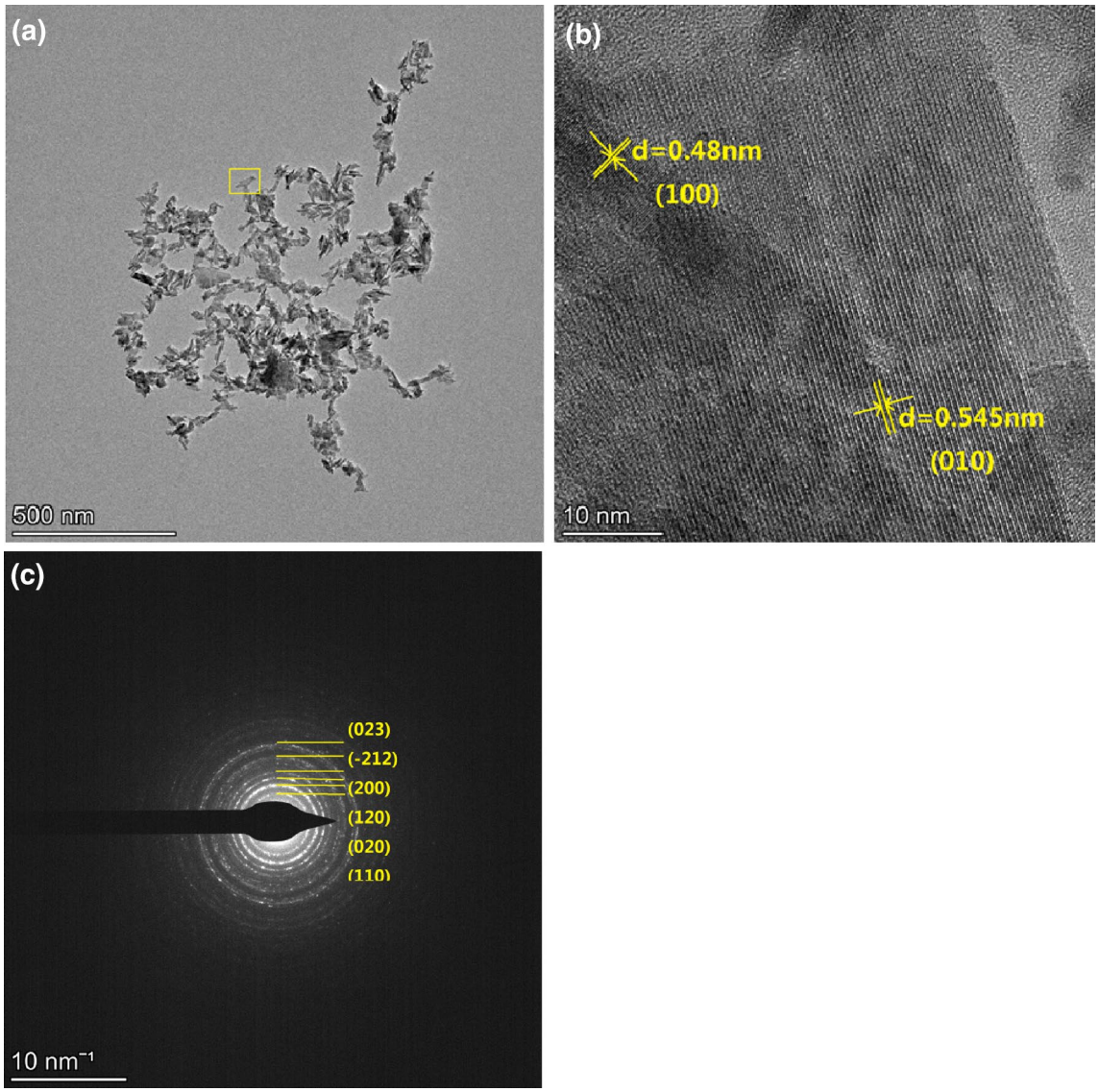

Fig. 2 **a** TEM image, **b** HRTEM image and **c** SAED pattern of $ZnWO_4$:0.07Eu^{3+} phosphors

represents indirect transitions are allowed, $t = 3$ stands for indirect forbidden transition, from the literature [18], the optical transition of $ZnWO_4$ is directly allowed, therefore where the value of t is 0.5, as presented in Fig. 4b. On the basis of the above Eq. (2), the optical band gap of pure $ZnWO_4$ and $ZnWO_4$:0.07Eu^{3+} phosphors were estimated to be 3.18 and 3.16 eV, respectively. As expected, the band gap values of $ZnWO_4$:0.07Eu^{3+} phosphors were lower than of the pure $ZnWO_4$ phosphor, indicating that the as-prepared $ZnWO_4$:0.07Eu^{3+} phosphors have a higher intrinsic electronic conductivity, and may be demonstrated that the superior electrochemical performances. In general, owing to rare earth ions doping, resulted in the impurity levels are formed, the result suggests that Eu^{3+} ions enter into the $ZnWO_4$ host. Confirming the $ZnWO_4$:0.07Eu^{3+} phosphors have a higher absorptive capacity than the $ZnWO_4$ host. In this figure, strong absorption band was observed at 350–490 nm, it was obviously observed that have one broad absorption band locating at 350–490 nm, which shows strong absorption ability located in 465 nm, at the same time, there is an obvious absorption peak, which point on the absorption spectrum corresponds to the 465 nm, deriving from the characteristic transition ($^7F_0 \rightarrow {}^5D_2$) of the Eu^{3+} [19].

3.5 Raman spectrum analysis

The structure of $ZnWO_4$ phosphor was further analyzed using the Raman spectrum, which is an effective way of studying the vibrational modes of lattices and molecules, there are a series of literatures [20] have reported that vibrational

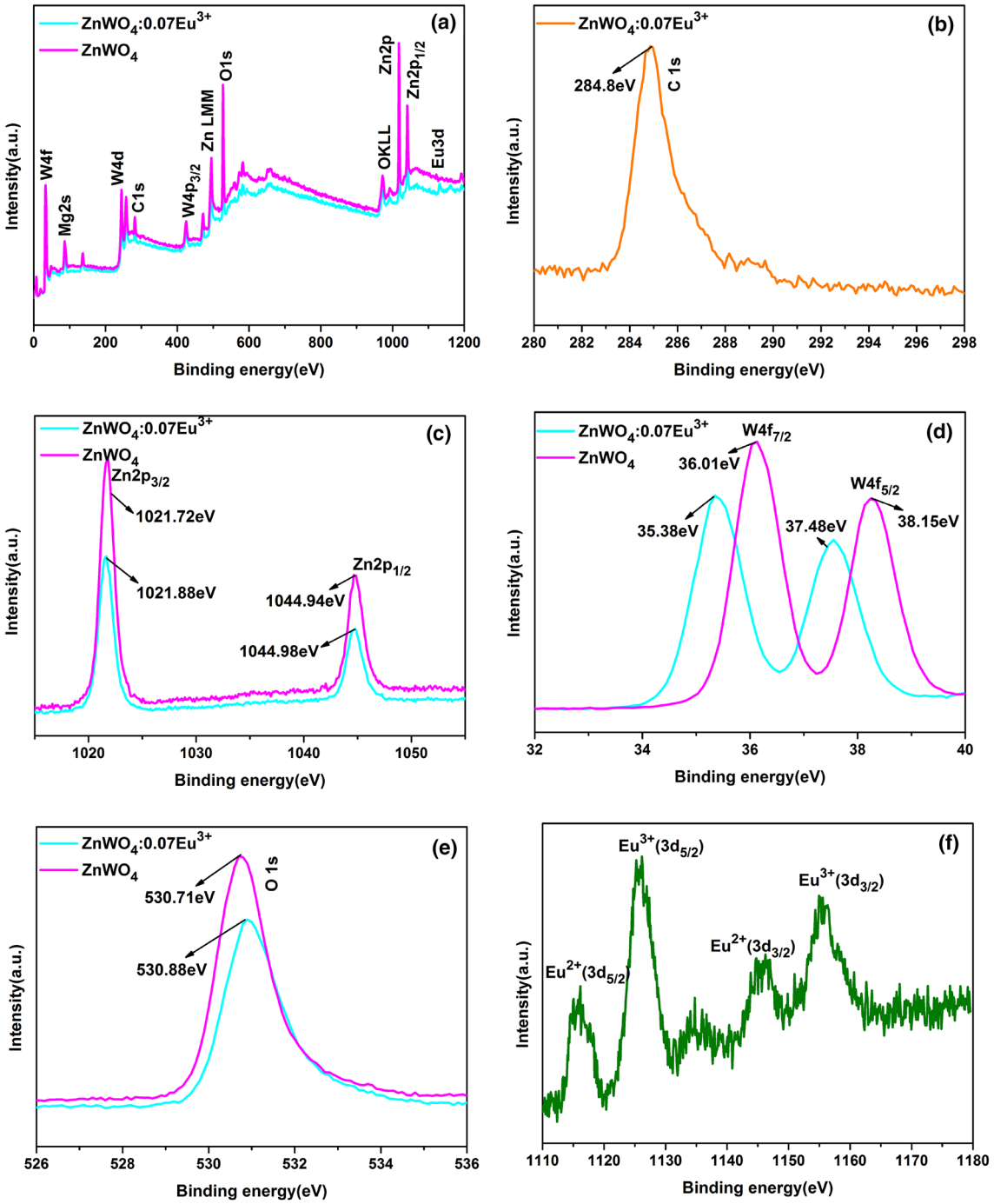

Fig. 3 XPS spectra of $ZnWO_4$:0.07Eu^{3+} for the chemical states of **a** broden spectra, **b** C, **c** Zn **d** W, **e** O and **f** Eu

modes of $ZnWO_4$ contain 36 patterns. The Raman spectrum is classified into external vibration and internal vibration mode, Raman activity parameters is A_g and B_g, and the optical. This can be formulated as follows:

$$\Gamma_{(\text{Raman})} = 8A_g + 10B_g \tag{3}$$

where g is Raman activity parameters, the Raman spectra of the $ZnWO_4$ was connected with other reports [21], and the pure peak can be observed prominent absorptions in the spectral range of 100–1000 cm^{-1} which correspond to six characteristic vibration patterns in Fig. 5. The bands at ~ 588 and 719 cm^{-1} are linking to symmetrical stretching vibrations connecting O atom in Zn–O–W [22], the two bands nearby 424 and 468 cm^{-1} are depicting into asymmetric

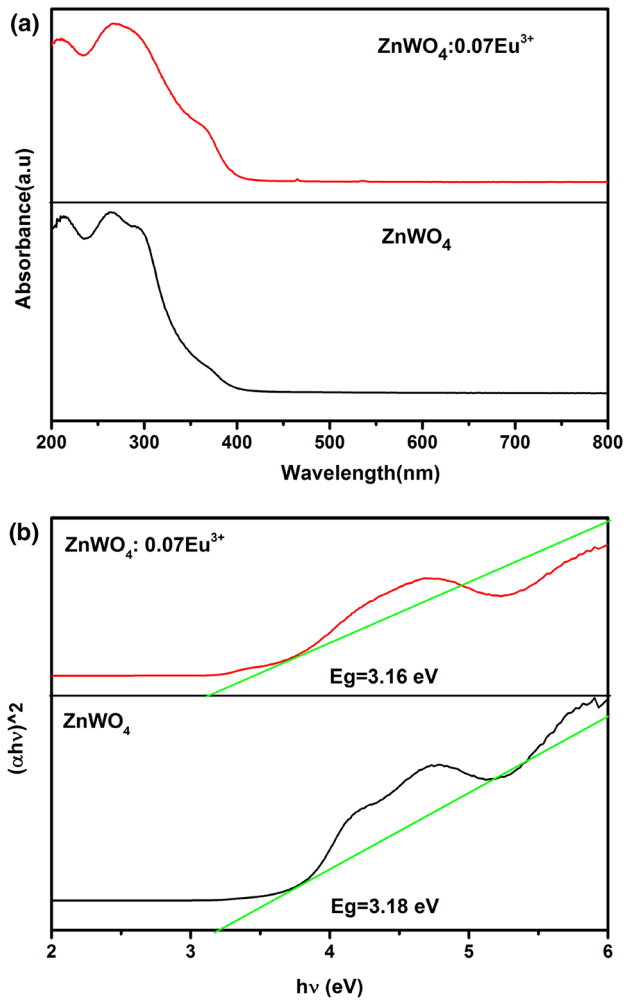

Fig. 4 **a** Ultraviolet–Visible reflectance absorption spectra **b** $(\alpha h\nu)^2$–$h\nu$ curves of the $ZnWO_4$ and $ZnWO_4$:0.07Eu^{3+}

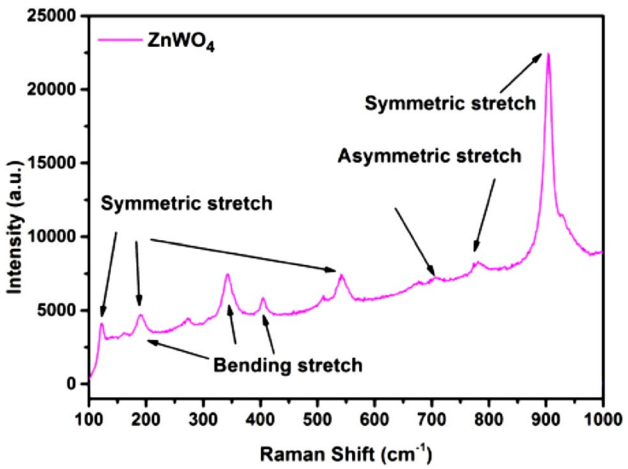

Fig. 5 Raman spectra of $ZnWO_4$ specimen

deformation of Zn–O and W–O in ZnO_6 and WO_6 octahedral ligand [23]. The two bands located at ~ 875 and 826 cm^{-1} were originating from the stretching pattern of WO_6 octahedron [24]. Raman spectrum was also completed to comprehend the influence of the doping. As displayed in Fig. 5, the relevant reports show the Raman shifts of the $ZnWO_4$ at 123, 141, 162, 190, 276, 320, 340, 405, 515, 542, 677, 709, 785 and 903 cm^{-1}, which explains this task. The three Raman bands located at ~ 123, 190 and 542 cm^{-1} can be described into the symmetric stretching of the ZnO_6 octahedron clusters, at the same time, the rest of the bands are a feature of the vibration pattern of WO_6 octahedron group. Vibration patterns are divided into internal and external modes. The internal extension patterns of WO_6 octahedron group were expressly solved as six Raman bands for the A_{1g} symmetric extension (~ 903 cm^{-1}). The E_g (709 and 785 cm^{-1}) and T_{2g} ($2A_g + B_g$, ~ 405, 340 and 190 cm^{-1}) were corresponding to asymmetric stretching and bending deformation of W–O bonds. The Raman band located at ~ 162 cm^{-1} was ascribed from the inter-chain torsion and distortion, however, that at ~ 276 cm^{-1} might be named as distortion vibration (A_g) of cationic sub-lattice of WO_6 octahedron group [25]. In addition, bands in the 500–600 cm^{-1} range are connected with W–O–W symmetric extension and the other located at ~ 141, 320 and 677 cm^{-1} are corresponding to the external vibration pattern of WO_6 octahedron cluster movement against Zn^{2+} [26]. The pure rod-like $ZnWO_4$ shows the strongest Raman, due to larger aspect ratio, hence led to the stronger Raman peaks [27]. Furthermore, the flexural vibration of the WO_6 octahedron group (190 cm^{-1}), locating at ~ 190 cm^{-1} originating from the symmetric extension vibration of ZnO_6 octahedron group, which verified that pure $ZnWO_4$ host with higher lattice symmetry, because no other defects were created $ZnWO_4$ the crystal structure. As shown in figure, the samples have to turn into the high band, when the Eu^{3+} occupy the Zn^{2+} of the $ZnWO_4$ host lattice, resulting in the distortion of the lattice. That could be caused by the small lattice and the offset of the Raman. In the internal vibration modes, Zn–O bonds are lower than the W–O bonds of the WO_6 octahedron group.

3.6 Photoluminescence (PL) analysis

The excitation spectrum of $ZnWO_4$:0.07Eu^{3+} phosphors were obtained by monitoring the emission wavelength at 616 nm, as displayed in Fig. 6a. The emission spectra can be observed the characteristic emission peaks of the Eu^{3+} [28], located in 594, 616, 654 and 705 nm, which originated from the transition of Eu^{3+}, corresponding to the transition of $^5D_0 \rightarrow {}^7F_1$, $^5D_0 \rightarrow {}^7F_2$, $^5D_0 \rightarrow {}^7F_3$, $^5D_0 \rightarrow {}^7F_4$, respectively [29]. Electron transition $^5D_0 \rightarrow {}^7F_2$ is predominant, when the transition intensity of the $^5D_0 \rightarrow {}^7F_2$ higher than the transition intensity of the $^5D_0 \rightarrow {}^7F_1$, suggesting

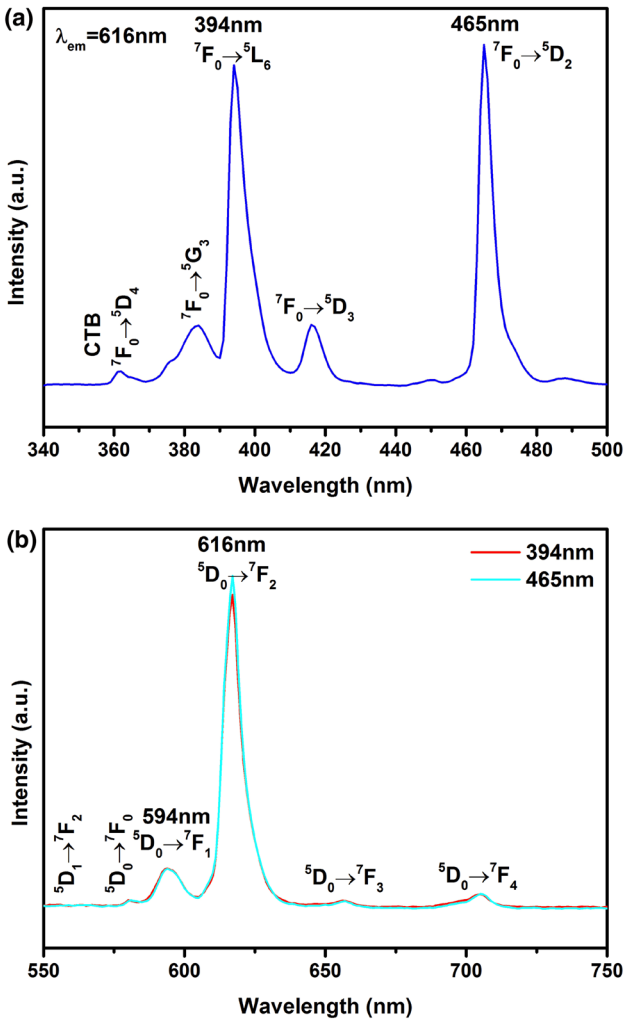

Fig. 6 **a** Excitation spectrum of $ZnWO_4$:0.07Eu^{3+} phosphors and **b** emission spectrum of $ZnWO_4$:0.07Eu^{3+} phosphors under diverse excitation

the Eu^{3+} ions occupy the asymmetric site of the lattice and no inversion center. Under the 616 nm emission spectra, in the wavelength wide range of 340–500 nm, it can be found that the suitable amount of purity in the products may produce some defects to become the new luminescent center, which is favorable for the luminescence of $ZnWO_4$:0.07Eu^{3+} phosphors.

Figure 6b displays the emission spectra of $ZnWO_4$:0.07Eu^{3+} phosphors under the excitation of 394 and 465 nm. It is interestingly to find the strongest intensity that was observed under 465 nm excitation, as shown in figure, all samples consist of the characteristic peak of the Eu^{3+}, the peaks center at 594 and 616 nm, originating from the $^5D_0$ state, and can be assigned to the magnetic dipole transition of Eu^{3+} ($^5D_0 \rightarrow {}^7F_1$) [30] and electric dipole transition of Eu^{3+} ($^5D_0 \rightarrow {}^7F_2$) [31], respectively. The weaker peaks at 654 nm, caused by the characteristic transition of

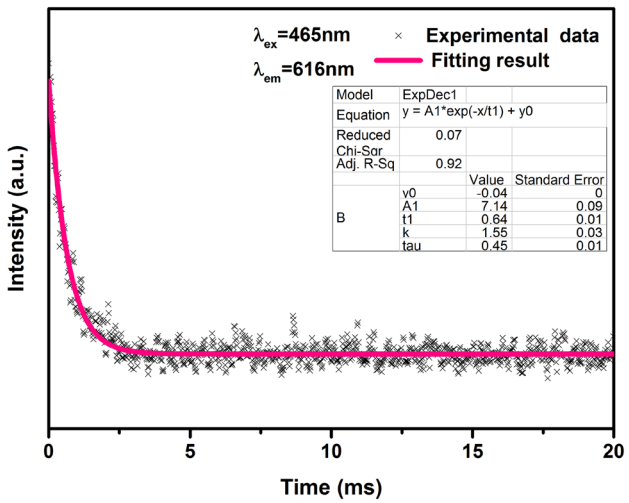

Fig. 7 The fluorescence decay of $ZnWO_4$:0.07Eu^{3+} phosphors

the Eu^{3+} ions ($^5D_0 \rightarrow {}^7F_3$) [16], the peak located at 705 nm which was assigned as the characteristic transition of the Eu^{3+} ($^5D_0 \rightarrow {}^7F_4$).

3.7 Lifetime analysis

The single exponential fitting decay curve of $ZnWO_4$:0.07Eu^{3+} phosphors were illustrated in Fig. 7. All decay life curves could be well fitted into first order exponential decay model function, and the single exponential fitting decay can be calculated by following formula [32]:

$$I(t) = I_0 + A\exp(-t/\tau) \quad (4)$$

where $I(t)$ is fluorescent intensity at time t, $I(0)$ is the background intensity, A is the constant, τ is the lifetime, the single exponential decay model of the phosphor was mainly due to Eu^{3+}-doped phosphors have same coordination environment into the host lattice and only exist in one deactivation process, the decay lifetime of the phosphor is 0.64 ms.

3.8 Electronic energy level scheme analysis

Figure 8 shows schematic diagram of energy level transitions of Eu^{3+} under excitation of 394 nm, excited by ultraviolet light 394 nm, Eu^{3+} ions were excited from $^7F_1$ to $^5D_2$ level and released to $^5D_0$ state were called the way of the non-radiative process. Eu^{3+} absorbed the photon energy from the ground state return to $^5L_6$, the energy was absorbed by the phosphors which emit non-radiative process will be dispersed to the crystal lattice. When $^5D_0$ has dwelled, Eu^{3+} ions display efficient visible emissions because of the multi-channel transitions. The sensitivity or the effect of ligand ion strongly on the emission intensity of the $^5D_0 \rightarrow {}^7F_2$ transition

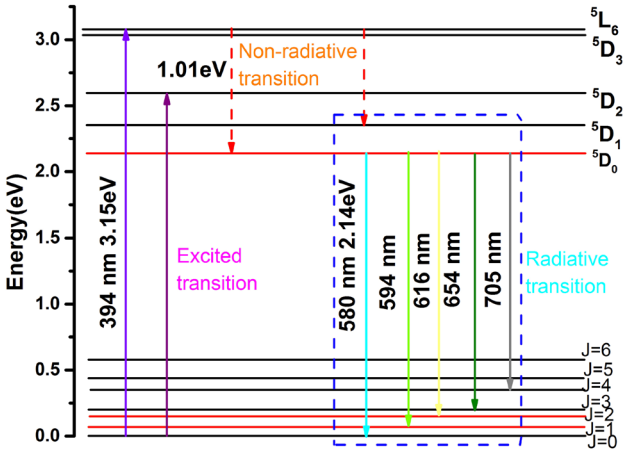

Fig. 8 Electronic energy level scheme of Eu^{3+} excited under 394 nm excitation

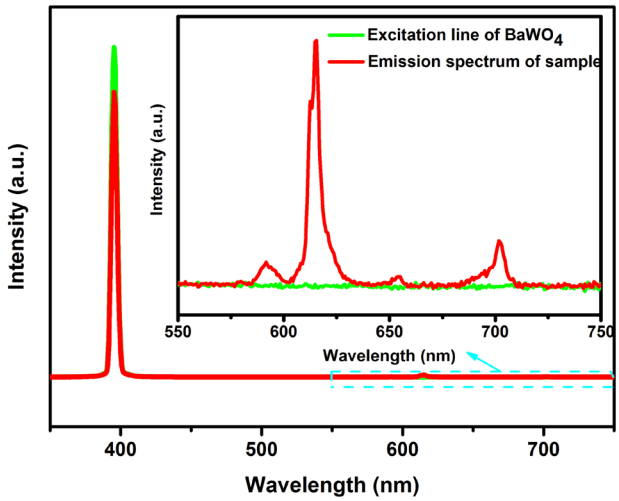

Fig. 9 Quantitative excitation and emission spectra of the $ZnWO_4$:0.07Eu^{3+} and $BaWO_4$ sample

is a target to study the local site symmetry of Eu^{3+} ions in the crystal lattice. Based on the above analysis, the symmetry site was occupied by the Eu^{3+} ions, therefore the electric dipole transition suggests that Eu^{3+} ions were located at an asymmetric site without an inversion center. There are peaks located at 594, 616, 655 and 702 nm that corresponding to the radiative transition of the $^5D_0 \rightarrow {}^7F_1$, $^5D_0 \rightarrow {}^7F_2$, $^5D_0 \rightarrow {}^7F_3$ and $^5D_0 \rightarrow {}^7F_4$ respectively. The corresponding photon energy can be obtained by calculating the photon energy equation [33]:

$$E = h\nu = \frac{hc}{\lambda} \tag{5}$$

where E is the photon energy, h is the Planck's constant, ν is the frequency of light, c is the vacuum speed of light, the value of c is 3.0×10^8 m/s, λ is excitation and emission wavelength. The energy of the non-radiative transition was released up to 1.01 eV.

3.9 The quantum efficiency (QE) and thermal stabilities of the phosphor analysis

The quantum efficiency is one of a key parameter used to be estimated the practical application, under the 394 nm excitation, the quantum efficiency $ZnWO_4$:0.07Eu^{3+} phosphors were measured with a Quantum-QY Plus UV–NIR absolute PL quantum yield spectrometer (C9920-03, Hamamatsu photonics K.K., Japan) with samples in powder form, and reference sample is $BaWO_4$ was illustrated in Fig. 9. The instrument is composed of photonic multi-channel analyzer PMA-12 (the detector) and PLQY measurement software-PMA as well as the photonic multi-channel analyzer (C10028) with the addition of supplementary units, which contains an excitation laser unit and a filter unit (A10094). The test measurements were measured at room temperature.

The quantum efficiency of the phosphors can be obtained as will see in the following the formula [34]:

$$\Phi_{PL} = \frac{N(\mathrm{Em})}{N(\mathrm{Abs})} = \frac{\int \frac{\lambda}{hc}\left[I_{em}^{sample}(\lambda) - I_{em}^{reference}(\lambda)\right] d\lambda}{\int \frac{\lambda}{hc}\left[I_{ex}^{reference}(\lambda) - I_{ex}^{sample}(\lambda)\right] d\lambda} \tag{6}$$

N(Abs) respects the number of photons absorbed of the sample, where N(Em) is the number of photons emitted from a sample, λ is the wavelength, h is Planck's constant and the value of h is 6.63×10^{-34} J·s, c is the velocity of light and the value is equal to 3×10^{17} nm/s, I_{ex}^{sample} represents the integrated intensities of the excitation light with sample, however, $I_{ex}^{reference}$ means integrated intensities of the excitation light without a sample, I_{em}^{sample} and $I_{em}^{reference}$ are the photoluminescence intensities with and without a sample, respectively. Based on the above test, the Quantum efficiency value of $ZnWO_4$:0.07Eu^{3+} phosphors were calculated to be 40.5%. In recent years, for most of the phosphors, Quantum yield of phosphors were further improved in practical applications via adjusting the reaction conditions and the amount Eu^{3+} ions doping.

Figure 10 depicts thermal stabilities of the $ZnWO_4$:0.07Eu^{3+} phosphors, the thermal stability is an important parameter for phosphors in WLEDs. Generally speaking, the temperature of the phosphors have an influence on thermal stability, attaching to its great influence on the efficiency of the phosphors. Integrated intensity of Eu^{3+} ions as a function of increasing temperature were depicted in Fig. 10. The integrated intensity of $ZnWO_4$:0.07Eu^{3+} phosphors gradually declines, when the temperature changes from 180 to 300 °C, and dramatically decreases above 220 °C, it was mainly due to the thermal

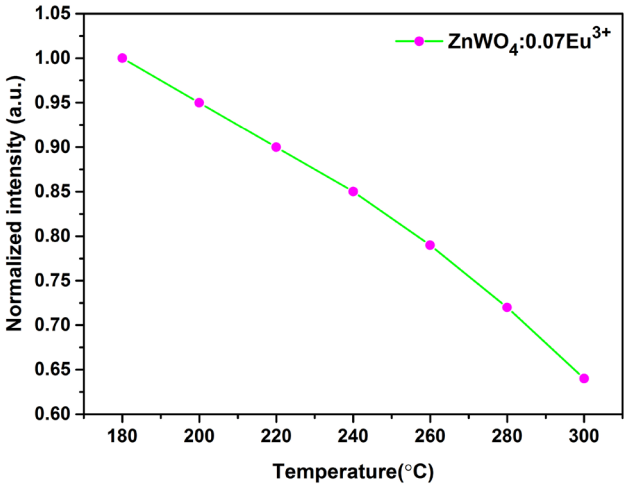

Fig. 10 Integrated intensity of Eu^{3+} ions as a function of increasing temperature

quenching, then it remains 90% of its initial intensity at 220 °C and reserves 85% at 240 °C. To further analysis the phosphor's thermal stability, the activation energy can be calculated by the Arrhenius equation as follows [35]:

$$I_T = \frac{I_0}{1 + D\exp\left(-\frac{E_a}{KT}\right)} \tag{7}$$

where I_0 and I_T represents the initial luminescence intensity and intensity at testing temperature and at different room temperature, respectively. D denotes a constant for a certain matrix, k is the Boltzmann constant and the value of k is 8.629×10^{-5} eVK^{-1}, E_a is activation energy of the thermal quenching, based on the above Eq. (7), the activation energy E_a of $ZnWO_4$:0.07Eu^{3+} phosphors were calculated to be 0.578 eV. In comparison with $CaGd_4F_{14}$:Ce^{3+} phosphor and Y_2MoSiO_8:Eu^{3+} phosphor. According to the literature [36, 37], the activation energy (E_a) of $CaGd_4F_{14}$:Ce^{3+} phosphor and Y_2MoSiO_8:Eu^{3+} phosphor are 0.503 and 0.29 eV, respectively. $ZnWO_4$:0.07Eu^{3+} phosphors have higher thermal stability, suggesting that it has better potential for indoor application of WLED [38].

3.10 Color coordinates analysis

Under the control of annealing temperature, upon the excitation by near ultraviolet light CIE chromaticity coordinates of the Eu^{3+}-doped $ZnWO_4$ phosphors were studied in Fig. 11. It is generally recognized that the color purity was calculated by the coordinate weighted average value relative to the light source point and the main control wavelength point, the formula is as follows [39]:

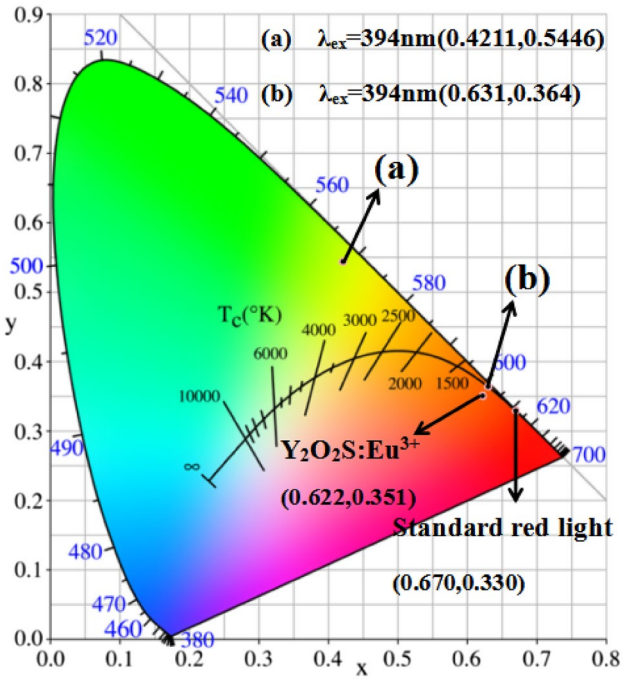

Fig. 11 CIE chromaticity diagram for the $ZnWO_4$:0.07Eu^{3+} phosphors **a** $ZnWO_4$ and **b** $ZnWO_4$:0.07Eu^{3+}

$$\text{Color purity} = \sqrt{\frac{(x - x_i)^2 + (y - y_i)^2}{(x_d - x_i)^2 + (y_d - y_i)^2}} \tag{8}$$

where (x, y) is color coordinate of phosphor light source, (x_i, y_i) is standard white light source color coordinates, (x_d, y_d) is the main emission coordinate of the emission spectrum, correlation color temperature is also an important parameter to measure the quality of light source, correlation color temperature was described as the following equation [40]:

$$\text{CCT} = -449n^3 + 3525n^2 - 6823.3n + 5520.33 \tag{9}$$

$$n = \frac{x - x_e}{y - y_e} \tag{10}$$

where the value of (x_e, y_e) is (0.3320, 0.1858), (x, y) represents color coordinates of phosphors. The parameters of the above were represented, the relevant result was summarized as follows in Table 1. In this work, it is well known that it

Table 1 Fluorescence parameters of $ZnWO_4$ and $ZnWO_4$:0.07Eu^{3+} phosphors under 394 nm excitation

X (mol %)	λ_{ex} (nm)	CIE (x, y)	CCT (K)	Color purity
0	394	(0.4211, 0.5446)	4025	66.08%
0.07	394	(0.631, 0.364)	2076	85.85%

has important applications in the white light field of solid-state lighting. CIE standard white light source is the (0.33, 0.33). In this paper, color coordinate of $ZnWO_4$:0.07Eu^{3+} phosphors were calculated is (0.631, 0.364) which is close to that of the NTSC standard CIE chromaticity coordinate value for (0.67, 0.33) and better than that of the commercial red Y_2O_2S:Eu^{3+}, the color coordinates of $ZnWO_4$:0.07Eu^{3+} phosphors are closer to the standard red light region. Therefore, in comparing with doping or un-doping, it is interestingly found that the color purity of the phosphor was improver than un-doping the $ZnWO_4$ host. It was suggested that $ZnWO_4$:0.07Eu^{3+} phosphors were applied in red-emitting phosphor as the next candidate for WLED.

3.11 Judd–Ofelt theory analysis

The theory can be used to explain the relationship between transition and relative intensity, which has become a powerful tool to study the luminescent properties of ions doping in solid-state lighting, it also provides information about the structural environment of metal ions and the chemical bonds of ions. According to the literature [41], the electric dipole transition intensity can be calculated the value of strength parameters Ω_λ ($\lambda = 2, 4, 6$), there are two transition modes for Eu^{3+}-doped the phosphors, one pattern is magnetic dipole transition of the $^5D_0 \rightarrow {}^7F_1$, another mode is electric dipole transition, the magnetic dipole transition probability was expressed as follows [12]:

$$A_{R(mo)} = \frac{64\pi^4\xi^3 n^3 S_{md}}{3h(2J+1)} \tag{11}$$

The S_{md} mean magnetic dipole line oscillator strength, the value of S_{md} is 7.83×10^{-42} esu^2 cm^2, it is a constant and isn't change with the substrate, where n is index of refraction of the host, h is Planck constant, ξ is average number of transitions, $^5D_0 \rightarrow {}^7F_J$ corresponding to the electric dipole transition (J = 2, 4, 6), the radiative transition probability was calculated by following formula [42]:

$$A_{(JO)} = \frac{64\pi^4 e^2 \xi^3}{3h(2J+1)}\varepsilon \sum_{\lambda=2,4,6} \Omega_\lambda \left\langle \psi J \left\| U^\lambda \right\| \psi' J' \right\rangle^2 \tag{12}$$

where e is the unit charge, ε is the refraction factor and the value of ε is $\varepsilon = n(n^2+2)^2/9$, $<\psi J\|U^\lambda\|\psi' J'>^2$ represents reduce the square of the matrix elements. The data of reduced matrix element was listed in Table 2. On the basis of the uniqueness of Eu^{3+}, strength parameters Ω_λ originated from $^5D_0 \rightarrow {}^7F_\lambda$ ($\lambda = 2, 4, 6$), therefore $A_{(JO)}$ shown by the following:

$$A_{(JO)} = \frac{64\pi^4 e^2 \xi^3}{3h(2J+1)} \frac{n\left(n^2+2\right)^2}{9} \Omega_\lambda \left\langle \psi J \| U\lambda \| \psi' J' \right\rangle^2 \tag{13}$$

Table 2 The data of reducing matrix element Eu^{3+} $^5D_0 \rightarrow {}^7F_{2,4,6}$ transitions

	$J=2$	$J=4$	$J=6$
$U^{(2)}$	0.0032	0	0
$U^{(4)}$	0	0.0023	0
$U^{(6)}$	0	0	0.0002

The ratio of the emission peak area corresponding to the transition of the $^5D_0 \rightarrow {}^7F_J$ (J = 2, 4, 6) to the emission peak area corresponding to the transition from $^5D_0 \rightarrow {}^7F_1$, which is the intensity ratio of electric and magnetic dipole transitions as following equation [43]:

$$\frac{A_{(JO)}}{A_{R(mo)}} = \frac{\int I_{(JO)} d\lambda}{\int I_{(mo)} d\lambda} \tag{14}$$

As mentioned in figure, the transition of the $^5D_0 \rightarrow {}^7F_6$ was not observed in the emission spectrum, so the value of the $^5D_0 \rightarrow {}^7F_6$ transition is equal to zero, radiation lifetime τ, lifetime contains radiative transition probability and non-radiative transition probability [44], the equation is shown as follows:

$$\frac{1}{\tau} = A_R + A_N \tag{15}$$

where A_R is the radiative transition, $A_R = \sum A_J$ (J = 0, 1, 2, 3, 4), the quantum efficiency was calculated as follows [45]:

$$\eta = \frac{1}{A_R + \frac{A_N}{A_R}} \tag{16}$$

The ratio of η is radiative transition probability to the total radiative transition probability. The stimulated cross-sectional area (σ_e) of the sample was studied, it's a measure which used to judge the laser performance of materials, the formula is expressed as follows [46]:

$$\sigma_e(\lambda_p) = \left(\frac{\lambda_p^4}{8\pi c n^2 \Delta\lambda_{eff}}\right) A_R \tag{17}$$

λ_p means the wavelength of emission peak, C is for the speed of light, $\Delta\lambda_{eff}$ is the effective bandwidth, the effective bandwidth is shown the equation [47]:

$$\Delta\lambda_{eff} = \int \frac{I(\lambda)\, d\lambda}{I_{max}} \tag{18}$$

Table 3 shows some J–O parameters of Eu^{3+} ions in the diverse host, in comparison with the context, it can also be observed that the quantum efficiency of our powders were higher than other matrices, which indicated the radiative transition probability of Eu^{3+} ions in $ZnWO_4$ phosphors were larger. Therefore $ZnWO_4$:Eu^{3+} phosphors may manifest the higher luminescent efficiency.

Table 3 Comparison of the intensity parameters (Ω_2, Ω_4), radiative transition probability (A_R), radiative lifetime (τ) and quantum efficiency (η) of Eu^{3+}-doping diverse host

Host matrix	Eu^{3+} (mol%)	Ω_2 (pm^2)	Ω_4 (pm^2)	A_R (s^{-1})	A_N+A_R (s^{-1})	η (%)	
$ZnWO_4$	7	3.51	1.08	1124.35	1605.08	70.08	Present
$SrLaEuLiTeO_6$	10	9.33	0.67	700	1282	55.0	[48]
$Sr_{0.8}Li_{0.2}T_{i0.8}Nb_{0.2}O_3$	8	3.60	1.59	707	1210	58.9	[49]
Nd_2ZrO_7	5	1.45	0.78	240	606	39.5	[50]

Table 4 Effective bandwidth of the emission transition ($\Delta\lambda_{eff}$), stimulating emission cross-section (σ_e) and gain bandwidth for $ZnWO_4$:0.07Eu^{3+} phosphors

Eu^{3+} (mol%)	Transitions	$\Delta\lambda_{eff}$ (nm)	σ_e ($\times 10^{-22} cm^2$)	$\sigma_e \times \Delta\lambda_{eff}$ ($\times 10^{-29} m^3$)
7	$^5D_0 \rightarrow {}^7F_1$	11.59	30.28	3.51
	$^5D_0 \rightarrow {}^7F_2$	11.98	40.67	4.87
	$^5D_0 \rightarrow {}^7F_4$	12.60	36.46	4.59

Based on the theoretical calculation, when the temperature is 180 °C, the intensity parameter Ω_2 value of $ZnWO_4$:Eu^{3+} phosphors are 3.509×10^{-20} cm^2, it can be observed the intensity parameters of $ZnWO_4$:0.07Eu^{3+} crystal continues to increase. At the same time, the intensity parameter Ω_4 of $ZnWO_4$:Eu^{3+} phosphors are 1.080×10^{-20} cm^2, respectively, the transition of $^5D_0 \rightarrow {}^7F_4$ is very weak in the spectra. It is concluded that Ω_4 is insensitive to the symmetry of its surroundings. All parameters were calculated in Table 3. The higher quantum efficiency indicates that the phosphors have better luminescent properties.

All relevant parameters were collected in Table 4, it can be seen that the excitation cross-sectional area corresponding to the electric dipole transition from $^5D_0 \rightarrow {}^7F_2$ of phosphors had a larger value. The larger stimulated cross-section area is more favorable for the laser with high gain, the luminescent performance of the phosphors are longer and better. Indicating that the transition of $^5D_0 \rightarrow {}^7F_2$ provides a good laser effect, more widely have potential applications in the optical display devices.

4 Conclusion

In this paper, we propose molten salt method-based hydrothermal reaction methods which makes principled use of Eu^{3+} doping. The Eu^{3+}-doped $ZnWO_4$:0.07Eu^{3+} phosphors have been successfully fabricated by the molten salt method. Under the excitation of 394 and 465 nm, the phosphors can be effectively excited. By introducing the Eu^{3+} ions into the $ZnWO_4$ matrix, quantum efficiency can be obtained enhance. It is usually accepted that the intrinsic characteristics have influence on the fluorescent properties. Based on the above calculated results, the chromaticity coordinates of $ZnWO_4$:0.07Eu^{3+} phosphors are (0.631, 0.364), the chromaticity coordinates of standard red phosphor is (0.67, 0.33), which suggests that $ZnWO_4$:0.07Eu^{3+} phosphors locate in the red region, on the basis of calculating the J–O parameters ($\Omega_2 > \Omega_4$), denoting that Eu^{3+} ions occupy the lowest symmetric of the phosphor. To the best of our knowledge, we are the first to use the molten salt method for studying quantum efficiency and stabilities properties in $ZnWO_4$:0.07Eu^{3+} phosphors. Therefore $ZnWO_4$:0.07Eu^{3+} phosphors can become a potential phosphor in WLEDs.

Acknowledgements This work was supported by the Projects for Science and Technology of Shaanxi province (No. 2019GY-175); Program for Scientific Research of Education Department of Shaanxi province (No. 18JK0111). We would like to thank the Testing Center of the Shaanxi University of Science& Technology. We sincerely thank Jianpeng Wu, Senior Engineer of the Shaanxi University of Science& Technology, for his help with XRD analysis and so on.

References

1. R.S. Yadav, S.J. Dhoble, S.B. Rai, Enhanced photoluminescence in Tm^{3+}, Yb^{3+}, Mg^{2+} tri-doped $ZnWO_4$ phosphor: three photon upconversion, laser induced optical heating and temperature sensing. Sens. Actuators B **273**, 1425 (2018)
2. S. Mamidi, R. Gundeboina, K. Sreenu, M. Vithal, Urea-modified $ZnWO_4$ with enhanced photocatalytic activity. J. Aust. Ceram. Soc. **54**, 671 (2018)
3. M.T. Li, T. Takei, Q. Zhu, B.-N. Kim, J.-G. Li, Morphology tailoring of $ZnWO_4$ crystallites architectures and photoluminescence of the doped RE^{3+} ions (RE = Sm, Eu, Tb, and Dy). Inorg. Chem. **58**, 9432 (2019)
4. M. Mohamed Jaffer Sadiq, S. Mutyala, J. Mathiyarasu, D. Krishna Bhat, RGO/$ZnWO_4$/Fe_3O_4 nanocomposite as an efficient electrocatalyst for oxygen reduction reaction. J. Electroanal. Chem. **799**, 102 (2017)
5. Z. Xia, J. Zhuang, L. Liao, Novel red-emitting $Ba_2Tb(BO_3)_2Cl$: Eu phosphor with efficient energy transfer for potential application in white light-emitting diodes. Inorg. Chem. **51**, 7202 (2012)
6. Y. Dang, X.J. Wang, R.R. Cui, S.L. Chen, Y.Z. Zhou, A novel electrochemical sensor for the selective determination of hydroquinone and catechol using synergic effect of electropolymerized nicotinic acid film and Cd-doped $ZnWO_4$ nanoneedle. J. Electroanal. Chem. **834**, 196 (2019)
7. M.Z. Zhao, Y. Liu, S.Y. Ma, D. Liu, K. Wang, Investigation of energy transfer mechanism and luminescence properties in Eu^{3+} and Sm^{3+} co-doped $ZnWO_4$ phosphors. J. Lumin. **202**, 57 (2018)
8. G. Chen, F. Wang, J. Yu, H.S. Zhang, X. Zhang, Improved red emission by codoping Li^+ in $ZnWO_4$: Eu^{3+} phosphors. J. Mol. Struct. **1128**, 1 (2017)

9. X.N. Chai, J. Li, X.S. Wang, Y.X. Li, X. Yao, Upconversion luminescence and temperature-sensing properties of Ho^{3+}/Yb^{3+}-codoped $ZnWO_4$ phosphors based on fluorescence intensity ratios. RSC Adv. **7**, 40046 (2017)
10. C.Y. Li, X.D. Du, D. Yue, M.N. Wang, J.B. Huang, Z.L. Wang, Color changing from white to red emission for $ZnWO_4$: Eu^{3+} nanophosphors at different temperature. Mater. Lett. **171**, 27 (2016)
11. R. Zhua, Y.S. Zeng, S.C. Liang, Y. Zhang, Y.H. Qi, Y.F. Liu, Y.N. Lyu, Regulated morphology of ScF_3: Eu^{3+}, Bi^{3+} microcrystals: microwave assisted hydrothermal synthesis, structure and luminescence properties. J. Solid State Chem. **269**, 447 (2019)
12. Z.W. Zhou, W.W. Li, J.H. Song, B.C. Mei, G.Q. Yi, Y. Yang, Application of Judd–Ofelt theory in analyzing Nd^{3+} doped SrF_2 and CaF_2 transparent ceramics. J. Eur. Ceram. Soc. **39**, 2446 (2019)
13. B.-W. Xun, Y.-C. Tang, J.-Y. Chen, B.-P. Zhang, Enhanced resistance in $Bi(Fe_{1-x}Sc_x)O_3$–$0.3BaTiO_3$ lead-free piezoelectric ceramics: facile analysis and reduction of oxygen vacancy. J. Eur. Ceram. Soc. **39**, 4085 (2019)
14. L.B. Chang, G.Q. Zhu, Q.-U. Hassan, B.W. Cao, S.P. Li, Y.F. Jia, J.Z. Gao, F.C. Zhang, Q.Z. Wang, Synergetic effects of Pd^0 metal nanoparticles and Pd^{2+} ions on enhanced photocatalytic activity of $ZnWO_4$ nanorods for nitric oxide removal. Langmuir **35**, 11265 (2019)
15. V.V. Atuchin, E.N. Galashov, O.Y. Khyzhun, A.S. Kozhukhov, L.D. Pokrovsky, V.N. Shlegel, Structure and electronic properties of $ZnWO_4$ (010) cleaved surface. Cryst. Growth Des. **11**, 2479 (2011)
16. Y.-M. Pan, W. Zhang, Z.-F. Hu, Z.-Y. Feng, L. Ma, D.-P. Xiong, P.-J. Hu, Y.-H. Wang, H.-Y. Wu, L. Luo, Synthesis of Ti^{4+}-doped $ZnWO_4$ phosphors for enhancing photocatalytic activity. J. Lumin. **206**, 267 (2019)
17. G.-T. Xiong, W. Zhang, Z.-F. Hu, P.-J. Hu, Y.-M. Pan, Z.-Y. Feng, L. Ma, Y.-H. Wang, L. Luo, Photocatalytic activity of $ZnWO_4$ phosphors doped with Li impurities. J. Lumin. **206**, 370 (2019)
18. R.F. Gonçalves, E. Longo, A.P.A. Marques, M.D.P. Silva, L.S. Cavalcante, I.C. Nogueira, I.M. Pinatti, P.F.S. Pereira, M.J. Godinho, Structural investigation and photoluminescent properties of $ZnWO_4$: Dy^{3+} nanocrystals. J. Mater. Sci. Mater. Electron. **28**, 15466 (2017)
19. Y.Q. Zhai, M. Wang, Q. Zhao, J.B. Yu, X.M. Li, Fabrication and luminescent properties of $ZnWO_4$: Eu^{3+}, Dy^{3+} white light-emitting phosphors. J. Lumin. **172**, 161 (2016)
20. X. Wang, Z. Fan, H.H. Yu, H.J. Zhang, J.Y. Wang, Characterization of $ZnWO_4$ Raman crystal. Opt. Mater. Express **7**, 1732 (2017)
21. M.T. Li, Q.H. Meng, S.Y. Li, F. Li, Q. Zhu, B.-N. Kim, J.-G. Li, Photoluminescent and photocatalytic $ZnWO_4$ nanorods via controlled hydrothermal reaction. Ceram. Int. **45**, 10746 (2019)
22. G.B. Kumar, K. Sivaiah, S. Buddhudu, Synthesis and characterization of $ZnWO_4$ ceramic powder. Ceram. Int. **36**, 199 (2010)
23. F. Dkhilalli, S.M. Borchani, M. Rasheed, R. Barille, K. Guidara, M. Megdiche, Structural, dielectric and optical properties of the zinc tungstate $ZnWO_4$ compound. J. Mater. Sci. Mater. Electron. **29**(8), 6297 (2018)
24. P. Yadav, S.K. Rout, E. Sinha, Correlation between optical properties and environmental parameter of $ZnWO_4$ ceramic using complex chemical bond theory. J. Alloys Compd. **726**, 1014 (2017)
25. P.J. Mafa, B. Ntsendwana, B.B. Mamba, A.T. Kuvarega, Visible light driven $ZnMoO_4$/$BiFeWO_6$/rGO z-scheme photocatalyst for the degradation of anthraquinonic dye. J. Phys. Chem. C **123**, 20605 (2019)
26. S.H. Cao, C.F. Gao, Y. Lv, Y.J. Guo, Q. Liu, A novel BiOCl film with flowerlike hierarchical structures and its optical properties. Nanotechnology **20**, 1 (2009)
27. Y. Liang, P. Liu, H.B. Li, G.W. Yang, $ZnMoO_4$ micro-and nanostructures synthesized by electrochemistry-assisted laser ablation in liquids and their optical properties. Cryst. Growth Des. **12**, 4487 (2012)
28. X.C. Song, Y.F. Zheng, E. Yang, G. Liu, Y. Zhang, H.F. Chen, Y.Y. Zhang, Photocatalytic activities of Cd-doped $ZnWO_4$ nanorods prepared by a hydrothermal process. J. Hazard. Mater. **179**, 1122 (2010)
29. Y.S. Shi, J.G. Shi, C. Dong, Refinement and luminescent properties of $BaWO_4$: xSm^{3+} yellow phosphor by a low temperature molten salt method. Opt. Mater. **84**, 396 (2018)
30. J. Shen, Z.X. Wang, J. Zhou, X. Liu, W. Chen, Photoluminescence properties of NUV light excited $Ba(Mg_{1/3}Nb_{2/3})O_3$: Eu^{3+} red phosphor with high color purity. Ceram. Int. **45**, 11844 (2019)
31. S.Y. Cao, Q.J. Ning, C.L. Yu, C.J. Qiao, Y.S. Shi, R.C. Liu, $NaSr_2Nb_5O_{15}$: $0.03Eu^{3+}$ phosphors via the molten salt synthesis: morphology evolution and luminescence properties. J. Alloys Compd. **691**, 323 (2017)
32. G. Jia, D.B. Dong, C.Y. Song, L.F. Li, C.M. Huang, C.M. Zhang, Hydrothermal synthesis and luminescence properties of monodisperse $BaWO_4$: Eu^{3+} submicrospheres. Mater. Lett. **120**, 251 (2014)
33. Y.S. Shi, B. Quan, Q.J. Ning, S.Y. Cao, J.J. Shi, C. Dong, Photoluminescent properties and Judd–Ofelt analysis of novel $Na_{0.5}Sr_{0.25}NbO_3$: Eu^{3+} red phosphor with high quantum efficiency. Mater. Res. Bull. **101**, 363 (2018)
34. J.S. Zhong, M. Xu, D.Q. Chen, G.H. Xiao, Z.G. Ji, Novel red-emitting Sr_2LaSbO_6: Eu^{3+} phosphor with enhanced $^5D_0 \rightarrow {}^7F_4$ transition for warm white light-emitting diodes. Dyes Pigm. **146**, 272 (2017)
35. C. Zeng, Y.M. Hu, L.J. Wang, H.K. Liu, C.Y. Liu, H.W. Huang, New green-yellowish emitting fluoro-apatite compound phosphor $Ba_3TbK(PO_4)_3F$: Sm^{3+} with high thermal stability. J. Rare Earths **35**, 767 (2017)
36. Z.W. Gao, L. Zhao, J.Y. He, R.J. Yu, A novel green-emitting phosphor of Ce^{3+}-activated $CaGd_4F_{14}$ synthesis, high efficiency, and thermal stability. Powder Technol. **331**, 244 (2018)
37. G.Y. Dong, J.X. Zhao, M.D. Li, L. Guan, X. Li, A novel red Y_2MoSiO_8: Eu^{3+} phosphor with high thermal stability for white LEDs. Ceram. Int. **45**, 2653 (2019)
38. M. Choi, H. Choi, J. Ahn, Y.T. Kim, Material design for $Ge_2Sb_2Te_5$ phase-change material with thermal stability and lattice distortion. Sci. Mater. **170**, 16 (2019)
39. M. Nandimath, R.F. Bhajantri, J. Naik, Effect of Rhodamine 6G dye on chromaticity co-ordinates and photoluminescence properties of TiO_2/PMMA polymer nanocomposites for LED applications. J. Lumin. **207**, 571 (2019)
40. Q. Sun, S.Y. Wang, B.L.J. Devakumar, L.L. Sun, J. Liang, X.Y. Huang, Y.C. Wu, $CaYAlO_4$: Mn^{4+}, Mg^{2+} an efficient far-red-emitting phosphor for indoor plant growth LEDs. J. Alloys Compd. **785**, 1198 (2019)
41. Q.J. Ning, B. Quan, Y.S. Shi, Effect of alkali metal ions on the spectra of $CaZn_2(PO_4)_2$: Sm^{3+} phosphor analyzed by J-O theory. J. Lumin. **206**, 498 (2019)
42. G. Lifante, J.M. Mendivil, R. He, E. Cantelara, L. Ortega San Martínd, D. Sola, Transition probabilities of Er^{3+} ions in aluminosilicate glasses. J. Lumin. **203**, 305 (2018)
43. J.M. de Mendívil, G. Lifante, M.C. Pujol, M. Aguiló, F. Díaz, E. Cantelar, Judd-Ofelt analysis and transition probabilities of Er^{3+} doped $KY_{1-x-y}GdxLuy(WO_4)_{(2)}$ crystals. J. Lumin. **165**, 153 (2015)
44. C. Aleksandar, S. Stevan, M.D. Dramicanin, Luminescence intensity ratio thermometry and Judd-Ofelt analysis of TiO_2: Eu^{3+}. Opt. Mater. **85**, 261 (2018)
45. Y.S. Shi, C. Dong, J.J. Shi, Influence of different synthesis methods on structure, morphology and luminescent properties of BiOCl: Eu^{3+} phosphors and J-O analysis. J. Mater. Sci. Mater. Electron. **29**(1), 186 (2018)

46. T. Manohara, S.C. Prashantha, R. Naik, H. Nagabhushana, H.P. Nagaswarupa, K.S. Anantharaju, K.M. Girish, H.B. Premkumar, A benign approach for tailoring the photometric properties and Judd-Ofelt analysis of $LaAlO_3$: Sm^{3+} nanophosphors for thermal sensor and WLED applications. Sens. Actuators B **243**, 1057 (2017)
47. K. Nasser, V. Aseev, S. Ivanov, A. Ignatiev, N. Nikonorov, Optical spectroscopic properties and Judd-Ofelt analysis of Nd^{3+}-doped photo-thermo-refractive glass. J. Lumin. **213**, 255 (2019)
48. S.C. Lal, A.M. Aiswarya, K.S. Sibi, G. Subodh, Insights into the structure photoluminescence and Judd-Ofelt analysis of red emitting $SrLaLiTeO_6$: Eu^{3+} phosphors. J. Alloys Compd. **788**, 1300 (2019)
49. G. Jyothi, L.S. Kumari, K.G. Gopchandran, Site selective substitution and its influence on photoluminescence properities of $Sr_{0.8}Li_{0.2}Ti_{0.8}Nb_{0.2}O_3$: Eu^{3+} phosphors. Rsc Adv. **7**, 28438 (2017)
50. S.K. Gupta, C. Reghukumar, R.M. Kadam, Eu^{3+} lacal site analysis and emission characteristic of novel $Nd_2Zr_2O_7$: Eu^{3+} phosphor insight into the effect of europium concentration on its photoluminescence properties. Rsc Adv. **6**, 53614 (2016)